

MIT Open Access Articles

*Combined Surface Micropatterning and Reactive Chemistry
Maximizes Tissue Adhesion with Minimal Inflammation*

The MIT Faculty has made this article openly available. **Please share**
how this access benefits you. Your story matters.

Citation: Pereira, M. J., et al. "Combined Surface Micropatterning and Reactive Chemistry Maximizes Tissue Adhesion with Minimal Inflammation." *Adv Healthc Mater* (2013).

As Published: 10.1002/ADHM.201300264

Publisher: Wiley

Persistent URL: <https://hdl.handle.net/1721.1/134514>

Version: Author's final manuscript: final author's manuscript post peer review, without publisher's formatting or copy editing

Terms of use: Creative Commons Attribution-Noncommercial-Share Alike





Published in final edited form as:

Adv Healthc Mater. 2014 April ; 3(4): 565–571. doi:10.1002/adhm.201300264.

Combined surface micropatterning and reactive chemistry maximizes tissue adhesion with minimal inflammation

Maria J. N. Pereira,

Division of Biomedical Engineering, Department of Medicine, Center for Regenerative Therapeutics, Brigham and Women's Hospital, Harvard Medical School, Harvard Stem Cell Institute, Harvard-MIT Division of Health Sciences and Technology 65 Landsdowne St., Cambridge, MA 02139, USA; Biocant- Biotechnology Innovation Center, CNC-Center of Neurosciences and Cell Biology, University of Coimbra, 3004-517 Coimbra, Portugal

Dr. Cathryn A. Sundback,

Center for Regenerative Medicine, Massachusetts General Hospital, Harvard Medical School 55 Fruit St., Boston, MA 02114, USA

Dr. Nora Lang,

Departments of Cardiac Surgery, Children's Hospital Boston, Harvard Medical School 300 Longwood Av., Boston, MA 02115, USA

Dr. Woo Kyung Cho,

Division of Biomedical Engineering, Department of Medicine, Center for Regenerative Therapeutics, Brigham and Women's Hospital, Harvard Medical School, Harvard Stem Cell Institute, Harvard-MIT Division of Health Sciences and Technology 65 Landsdowne St., Cambridge, MA 02139, USA; Department of Chemical Engineering and the David H. Koch Institute for Integrative Cancer Research, Massachusetts Institute of Technology 500 Main Street, Cambridge, MA 02139, USA; Department of Chemistry, Chungnam National University, Daejeon 305-764, South Korea

Dr. Irina Pomerantseva,

Center for Regenerative Medicine, Massachusetts General Hospital, Harvard Medical School 55 Fruit St., Boston, MA 02114, USA

Ben Ouyang,

Division of Biomedical Engineering, Department of Medicine, Center for Regenerative Therapeutics, Brigham and Women's Hospital, Harvard Medical School, Harvard Stem Cell Institute, Harvard-MIT Division of Health Sciences and Technology 65 Landsdowne St., Cambridge, MA 02139, USA

Dr. Sarah L. Tao⁺,

Draper Laboratory Biomedical Engineering Center Mail Stop 32, 555 Technology Square, Cambridge, MA 02139, USA

Kevin McHugh,

^[*]Corresponding authors: Prof. Lino Ferreira, Prof. Jeffrey M. Karp, Dr. Peter T. Masiakos
lino@biocant.ptjkarp@rics.bwh.harvard.edupmasiakos@partners.org.

^[†]Current address: Cooper Vision, Pleasanton CA, USA

Draper Laboratory Biomedical Engineering Center Mail Stop 32, 555 Technology Square,
Cambridge, MA 02139, USA

Olive Mwizerwa,

Center for Regenerative Medicine, Massachusetts General Hospital, Harvard Medical School 55
Fruit St., Boston, MA 02114, USA

Dr. Praveen K. Vemula,

Division of Biomedical Engineering, Department of Medicine, Center for Regenerative
Therapeutics, Brigham and Women's Hospital, Harvard Medical School, Harvard Stem Cell
Institute, Harvard-MIT Division of Health Sciences and Technology 65 Landsdowne St.,
Cambridge, MA 02139, USA

Dr. Mark C. Mochel,

Department of Pathology, Massachusetts General Hospital 55 Fruit Street, Boston, MA 02114,
USA

Dr. David J. Carter,

Draper Laboratory Biomedical Engineering Center Mail Stop 32, 555 Technology Square,
Cambridge, MA 02139, USA

Dr. Jeffrey T. Borenstein,

Draper Laboratory Biomedical Engineering Center Mail Stop 32, 555 Technology Square,
Cambridge, MA 02139, USA

Prof. Robert Langer,

Department of Chemical Engineering and the David H. Koch Institute for Integrative Cancer
Research, Massachusetts Institute of Technology 500 Main Street, Cambridge, MA 02139, USA

Dr. Lino S. Ferreira*,

Biocant- Biotechnology Innovation Center, CNC-Center of Neurosciences and Cell Biology,
University of Coimbra, 3004-517 Coimbra, Portugal

Prof. Jeffrey M. Karp*, and

Division of Biomedical Engineering, Department of Medicine, Center for Regenerative
Therapeutics, Brigham and Women's Hospital, Harvard Medical School, Harvard Stem Cell
Institute, Harvard-MIT Division of Health Sciences and Technology 65 Landsdowne St.,
Cambridge, MA 02139, USA

Dr. Peter T. Masiakos*

Center for Regenerative Medicine, Massachusetts General Hospital, Harvard Medical School 55
Fruit St., Boston, MA 02114, USA

Abstract

The use of tissue adhesives for internal clinical applications is limited due to a lack of materials that balance strong adhesion with biocompatibility. The use of substrate topography was explored to reduce the volume of a highly reactive and toxic glue without compromising adhesive strength. Micro-textured patches coated with a thin layer of cyanoacrylate glue achieved similar adhesion levels to patches employing large amounts of adhesive, and was superior to the level of adhesion achieved when a thin coating was applied to a non-textured patch. In vivo studies demonstrated

reduced tissue inflammation and necrosis for patterned patches with a thinly coated layer of reactive glue, thus overcoming a significant challenge with existing tissue adhesives such as cyanoacrylate. Closure of surgical stomach and colon defects in a rat model was achieved without abdominal adhesions. Harnessing the synergy between surface topography and reactive chemistry enables controlled tissue adhesion with an improved biocompatibility profile without requiring changes in the chemical composition of reactive tissue glues.

Keywords

wet tissue adhesive; microtextured; biodegradable glue; bioinspired; biocompatibility

1. Introduction

Synthetic sutures, clips and staples are commonly used by surgeons to close surgical wounds, repair disrupted tissue and perform delicate gastrointestinal and vascular anastomoses. Although these materials have improved surgical care by decreasing operative times and providing secure tissue attachment, several limitations remain.^[1] Namely, unwanted tissue trauma and ischemia occur and, even in the hands of highly-trained surgeons, the process of suturing is time-consuming. Furthermore, suturing or stapling is challenging when procedures involve distant and small anatomic spaces. Sutures and stapling devices appear to have reached the limits of their application and next generation wound closure alternatives must be developed to advance minimally invasive surgery. Biodegradable tissue adhesives for internal use offer a potential solution to these problems. Ideally these tissue adhesives will support atraumatic defect closure and secure anastomoses of vessels or intestine while minimizing unwanted inflammation. However, introducing this technology into the clinic has been challenging due to the lack of materials that strongly adhere in wet environments and most induce an inflammatory response and are toxic. In this study, we describe a novel approach to tissue adhesion which synergistically combines microtopography and reactive chemistry to maximize adhesive strength and restrict inflammation.

Medical grade cyanoacrylates (CA) adhere strongly to tissue upon exposure to water or other basic compounds; however, they are associated with tissue toxicity.^[2, 3] Despite several attempts to improve its biocompatibility through changes in the CA chemical composition,^[4] their use has been essentially limited to external applications because of toxicity and inflammatory response concerns. These undesirable properties derive from the reactivity of CA towards functional groups on tissue surfaces, the exothermic nature of the bonding reaction and the degradation products of CA (e.g. formaldehyde and cyanoacetate).^[3-5] To overcome these issues, new approaches for tissue bonding are actively being pursued. Specifically, a growing body of work on bioinspired gecko-like adhesion has shown potential for achieving dry and wet adhesion.^[6-8] Our group previously developed an elastomeric biodegradable and biocompatible gecko- inspired tissue adhesive tape based on the combination of nanotopography and mild surface chemistry.^[7] A layer of dextran-aldehyde glue^[9] was used to coat the nanotextured surface, enabling adhesion in wet environments without a significant inflammatory response. Improved adhesion relative to

flat surfaces was attributed to greater tissue contact from the increased surface area of the nanotextured surface and to the presence of mechanical interlocking. However, the forces achieved using a mild surface chemistry coupled with nanotopography were not enough for some clinical applications.

Towards creation of more clinically relevant adhesives, we hypothesized that strong levels of adhesion could be achieved through the application of a small quantity of highly reactive tissue glue coated on patterned substrates. We selected medical grade CA as the reactive coating, whose toxicity has been demonstrated in several pre-clinical^[10] and clinical^[2] studies. To maximize tissue adhesion under wet conditions, we employed larger topographical features to allow thicker coatings without occluding the topography.

2. Results and discussion

Micron-scale topographies were prepared through reactive ion etching of a silicon wafer, which were used to create topographies that enhance tissue adhesion (Fig. SI 1). Unlike nanoscale substrate features that become obstructed with excess glue^[7], micron-scale topographies enable a thicker CA layer without compromising the morphology of the underlying microtextured substrate. Furthermore, previous reports have shown that microstructures effectively enhance the friction of materials against wet biological tissues.^[6,11] Here, we developed pillar arrays with different initial surface areas and geometries to evaluate the capacity to form thin patterned CA films upon spin coating (Fig. SI 1). We initially used PDMS as the substrate material, as it is easily and reproducibly patterned, elastic, and a model material extensively used for topography-adhesion testing.^[12] A pilot screening was performed that included the following design parameters: 1) robustness of the pillar to avoid collapse, 2) density of the pillars per surface area, and 3) height of the pillars to avoid CA occlusion of the space between the pillars in the patterned array. Upon spin coating with CA glue, the coated PDMS patch was immediately applied to wet intestine tissue. The patch in contact with tissue was allowed to cure for 5 minutes, followed by *in vitro* 90° pull-off adhesion measurements. A significant increase ($p < 0.05$ compared with other experimental conditions, according to a one-way ANOVA with the Tukey post-hoc statistical test) was observed in adhesion strength for one of the candidate topographies consisting of pillars spin coated with CA (base: 4.9 μm , height: 19.0 μm , pitch: 9.5 μm); no or minor adhesion strength increase was found with the other topographies (Fig. SI 1). This topography was selected for the subsequent studies.

To facilitate translation to medical applications, a biodegradable and biocompatible material, poly(ϵ -caprolactone) (PCL), was utilized as the substrate material. Multiple PCL products have been FDA-approved for internal application (e.g. biodegradable sutures) and its biocompatibility has been documented in many wound closure applications.^[13] Given its low melting temperature ($\sim 60^\circ\text{C}$), PCL can be easily patterned with high fidelity over large surface areas using hot embossing, which eliminates organic solvent use (Fig. 1A). The pillar of the hot embossed patterns had a height of $13.2 \pm 1.0 \mu\text{m}$, a base diameter of $5.15 \pm 0.4 \mu\text{m}$, and a pitch of $9.3 \pm 0.3 \mu\text{m}$. Upon spin-coating, the uniformity of CA-coated patterned PCL surfaces (Fig. 1B) was confirmed by measurements of the coating thickness at randomly selected patch locations through SEM fracture surfaces (Fig. SI 2). The coating

thickness at the base was approximately $2.6 \pm 1.4 \mu\text{m}$, and the observable patterns dimensions were $10.6 \pm 1.0 \mu\text{m}$ height and 5.4 ± 0.7 base diameter. *Ex vivo* 90° pull-off adhesion tests against wet intestine tissue confirmed that the topography enhanced the adhesion force of thin CA coatings on patterned patches compared to flat substrates (Fig. 1C). The adhesion force of CA spin-coated patterned substrates was similar to non-spin-coated flat or patterned PCL with excess CA ($5 \mu\text{L}$). Increasing the curing time of CA-coated patches in contact with tissue from 5 minutes (Fig. 1C) to 1 hour (Fig. SI 3) did not impact the trend of higher adhesion for patterned versus flat spin coated patches. Overall, our results show that the combination of microtopography with CA coating enhances patch adhesion. The mechanical properties and surface tension of PCL differ from the PDMS substrate used in the pilot screening experiments. It cannot be excluded that other topographies could behave differently when using PCL instead of PDMS and future work should focus on understanding the combinatorial effect of mechanical properties in pillar geometry requirements for maximal adhesion.

Surface patterning enhanced the hydrophobic nature of PCL surface, increasing the water contact angle from $96 \pm 4^\circ$ (flat surface) to $128 \pm 6^\circ$ (patterned surface) (Fig. 2A and B). These observations are consistent with previous studies which demonstrated the impact of substrate micropatterning on increasing hydrophobicity.^[14] To investigate the interface compatibility between CA and PCL, we deposited CA drops on flat and patterned surfaces and assessed their spreadability. CA spread more on patterned (angle of $12 \pm 4^\circ$), than on flat surfaces (angle $28 \pm 7^\circ$) (Fig. 2A and B). Spin-coating polymer solutions has been shown to be dependent on substrate wettability; enhanced wettability led to more uniform coating for a given surface topography.^[15] Therefore, greater spreadability of the hydrophobic CA is likely related to the enhanced hydrophobicity of the patterned surface. Chemical mapping was employed to evaluate spin-coated CA coverage of the pillar structures. Given the similar chemical compositions, iron oxide nanoparticles (IO) were encapsulated within CA to allow CA and PCL to be distinguished. IO did not interfere with the CA spin-coating process nor impact the thickness of the final glue layer (Fig 1B and 2C). EDX analysis confirmed that CA covered the pattern yet did not occlude the space between pillars. In SEM images, CA appeared to partially accumulate at the base of the pillars (Fig. 1B), which likely occurred prior to curing given the fluidity of CA prior to hardening.

The relative amounts of CA on spin-coated patterned substrates, flat substrates, and $5 \mu\text{L}$ non spin-coated substrates were quantified through Inductively Coupled Plasma - Atomic Emission Spectrometry (ICP-AES) based on the iron signal from the IO encapsulated within CA. Spin-coating CA on a flat substrate reduced the glue volume by 13 ± 2 times compared with the $5 \mu\text{L}$ CA applied without spin-coating. Spin-coated patterned substrates retained more CA than spin-coated flat substrates ($p < 0.05$) (Fig. 2D). However, given the greater surface area of the patterned substrates, the CA volume per unit surface area on the patterned samples was less than that of the flat substrate (~ 0.78 times); this observation suggested that the CA layer was likely thinner on patterned substrates than on flat substrates. Patterned PDMS substrates spin-coated with CA were evaluated by SEM following pull-off tensile testing from intestine tissue. These images revealed interlocking of tissue with the surface topography (Fig. 2E). Similar order of magnitude in increased surface area (~ 2.3

times, for PCL patch material) and increased adhesion strength (~2.6 times, Fig. 1C) were observed relative to patterned and flat spin-coated samples. From these data, enhanced adhesion may be related to the contact area increase for the patterned samples and/or the higher levels of CA in patterned samples.

In vivo biocompatibility experiments were performed to evaluate the impact of CA at the tissue-patch interface on the tissue response. CA coated PCL patches were subcutaneously implanted in rats and the tissue responses were evaluated after 1 and 3 weeks implantation using H&E and anti-CD 68 stains (Fig. 3A, B and C). The inflammatory reaction to patterned spin-coated samples was similar to that of patterned uncoated material at 1 week post-implantation; at 3 weeks post-implantation, higher levels of neovascularization and foreign body giant cells were observed. Markers of inflammation to uncoated material were unchanged at 3 weeks. Cell necrosis was observed in all CA-containing samples at 1 week post-implantation (spin-coated or 5 μ L) but only in the 5 μ L CA samples at 3 weeks post-implantation (Fig. 3B). Early cell necrosis may have been induced by the high reactivity of CA during covalent bonding to the tissue surface, while long-term necrosis may be related to the release of toxic CA degradation products. At both time points, more severe inflammatory responses and thicker fibrotic capsules were observed in samples coated with 5 μ L CA than in uncoated patterned and CA spin-coated samples; no statistical differences in inflammation or fibrotic capsule thickness were found between uncoated patterned and CA spin-coated samples (Fig. 3C). The histotoxicity of CA was highly dependent on the amount of glue applied to the tissue interface. Spin-coating reduced the amount of glue and its toxic products released during degradation.

The ability of spin-coated samples to functionally close gastrointestinal perforations was evaluated using rat models with colon or stomach puncture (Fig. 3D and 3E, respectively). Suturing is the current standard of care for defect closure. However, tissue edges are often thin and friable, leading to inefficient closure and leakage of the gastrointestinal contents into the abdominal cavity. The adhesion of flat or patterned spin-coated patches to the colon surface (Fig. 3D i) was graded by a single surgeon blinded to the topography, immediately after patch placement on the defect in the tissue. Statistically significant differences in the degree of adhesion were found, confirming improved sealing of patterned samples in comparison with flat spin-coated samples (Fig. 3D ii). Upon secure attachment, all patches remained in place for a minimum of 1 week. No major inflammatory response was observed surrounding the defect (Fig. 3D iii), confirming favorable biocompatibility in reduced CA samples.

Patterned spin-coated patches were also adhered to the stomach serosal surface, covering a 3 mm gastrotomy. These patches remained adherent for a minimum of 2 weeks (Fig. 3E i). Negative control sham surgeries were performed in which a gastrotomy was created but not repaired. As a positive control, the stomach defect was closed using a Graham patch technique, which is routinely used to close gastric perforations^[16]; the greater omentum, which is highly vascularized and contains progenitor cells that promote tissue repair^[17], was sutured over the defect. Two weeks following repair, minimal abdominal adhesions were observed when the stomach defect was closed with a spin-coated patterned patch, moderate or severe adhesions were found when Graham patch or sham operations were performed,

respectively (Fig. 3E ii). These data suggested that the PCL patch provided a functional seal of gastrointestinal perforations. The impact of the CA glue on the stomach mucosa was evaluated through H&E staining (Fig. 3E iii) of the tissue underlying the patch.

Inflammatory responses at tissue injury sites have been found to inhibit tissue repair and regeneration^[18]; however, defects covered with spin-coated patterned PCL patches demonstrated closure by 2 weeks post-repair.

3. Conclusions

Surface topography enhanced the effectiveness of thin adhesive coatings. Importantly, patch patterning reduced the CA amount at the tissue-patch interface, improving the biocompatibility of CA-coated patches without compromising adhesive strength. To our knowledge, this is the first demonstration that has correlated the CA amount applied to tissue with the observed histotoxic and inflammatory responses. Utilizing this concept, other glue delivery approaches may be developed to maximize CA adhesive strength, while minimizing induced toxicity. These approaches may expand the clinical applications that employ CA beyond external application procedures.

4. Experimental

Silicon micromolds fabrication

Silicon wafers with oxide layer approximately 2 μm thick were baked at 110°C to dehydrate their surface and spin-coated with hexamethyldisilazane at 5000 rpm for 10 seconds to promote resist adhesion. Photoresist (PR, Shipley 1805) was then spin-coated (EVG101, EVG) on the wafers at 3500 rpm for 20 seconds. The wafer was then softbaked on a hotplate at 115°C for 1 min to yield a resist film thickness of approximately 500 nm. Resist exposure was done with a Karl Suss MA-6 contact aligner with an exposure dose of 96 mJ/cm^2 , and the resist was developed for 45 seconds in Shipley MF-319 developer followed by a 3 minute rinse in deionized (DI) water and spin-drying. The PR micro-patterned silicon wafer was then treated with an oxygen plasma in a barrel asher (March Systems) for 30 seconds at a power of 55 W and a vacuum level of 250 mTorr. Micropatterns were transferred from the photoresist to the underlying oxide layer by reactive ion etching to generate the final micromold. In detail, a Multiplex Reactive Ion Etcher (Surface Technology Systems) was used to etch the oxide layer in CHF_3/CF_4 at gas flow rates of 14.4 and 1.6 sccm, respectively, at a pressure of 20 mTorr and RF power level of 200 W, resulting in an oxide etch rate of approximately 3 nm/second. After the etching, the PR layer was removed by immersing the substrate into acetone and SVC-12 (Microchem) for 30 min each, and EKC-270 stripper for up to 3 h. The substrate was then washed with DI water thoroughly for 10 min, and spin-dried.

Micropatterning and characterization of PDMS and PCL films

For PDMS patterning, a negative mold was initially prepared with acrylated polyurethane resin (PUA) through soft-lithography using the positive silicon mold, followed by surface treatment with (tridecafluoro-1,1,2,2-tetrahydrooctyl)trichlorosilane (TTT, Gelest). PDMS pre-polymer was poured onto the PUA mold, degassed under vacuum and cured overnight at

60°C. For PCL micropatterning, negative PDMS molds were fabricated directly from the silicon molds, followed by surface treatment with TTT. PCL (Mw= 43 000 - 50 000 g/mol, Polysciences) films were melted at 130°C on top of negative PDMS molds followed by compression against a Teflon plate to assure pattern transfer. PCL films were carefully removed after cooling. The efficiency of pattern transfer was evaluated through scanning electron microscopy (SEM, FEI/Phillips XL30 FEG-ESEM).

CA spin coating procedure of PDMS and PCL film

15 μ L of CA (Dermabond®, Medstarsutures) was spin-coated at 3000 RPM for 3 minutes on PDMS and PCL patterned or flat surfaces. CA coating thickness was determined through the analysis of SEM images obtained from cross-sections of coated and uncoated patterned surfaces (n=4 different substrates per experimental condition). The differences in height between non-coated and CA spin-coated pillars was used to determine the CA glue layer thickness. Figure SI 2 shows how the measurements were performed. The software ImageJ was used to calculate pillar dimensions.

Pull-off adhesion testing

90° Pull-off adhesion tests were performed using an ADMET eXpert 7601 universal tester, equipped with a 50 N load cell. Experimental conditions included i. micropatterned surfaces spin-coated with CA at 3000 RPM, ii. flat surfaces spin-coated with CA at 3000 RPM, iii. flat surfaces with 5 μ L of CA, or iv. patterned surfaces with 5 μ L of CA (n=3 per condition for PDMS substrates, n= 6 per condition for PCL substrates). 5 μ L of glue was applied to non-spin coated substrates as additional amounts of glue were easily displaced after application to tissue. To ensure uniform coating across the surface of spin-coated patches, 15 μ L of glue was applied. Immediately after CA coating, the samples were attached to the wet serosal side of porcine intestine tissue, previously immobilized on a flat metallic stub. Samples were cured for 5 min, or for 1 hour immersed in phosphate buffer saline, followed by pull off at 8 mm/min. Adhesion force was recorded as the maximum force observed during pull off testing. The contact area between tissue and adhesive was circular in shape with a diameter of 6 mm.

Characterization of CA-coated PCL surfaces

CA spreadability—The water contact angle for flat and patterned PCL surfaces was measured. The spreading of CA on flat and micropatterned PCL was evaluated through the application of a CA drop on patterned or flat PCL surfaces and examining the angle that formed (n=4 per condition).

Chemical mapping of CA glue layer—Energy-dispersive X-ray spectroscopy (EDX) was applied to visualize how CA covers the micropatterned surface. CA glue was mixed with iron oxide nanoparticles (IO, 10 nm, Oceananotech) functionalized with oleic acid for uniform dispersion, followed by spin-coating at 3000 RPM for 3 min on a patterned PCL surface. The encapsulation of IO does not interfere with the glue layer thickness, confirmed through SEM analysis. Data was collected at 25 kV using an X-ray detector coupled with FEI/Phillips XL30 FEG-ESEM. The iron signal could be easily detected and mapped through EDX.

CA quantification—Quantification of CA in flat versus patterned samples after spin-coating was performed through induced coupled plasma atomic emission spectroscopy (ICP-AES, ACTIVA-S Horiba Jobin Yvon). Patterned or flat patches spin-coated with CA-IO glue, or CA-IO glue only were solubilized in acetone. IO particles were isolated from the organic materials through sequential centrifugations and re-suspended in chloroform. Following chloroform evaporation, the IO nanoparticles were digested in *aqua regia*, which was then evaporated, and re-suspended in aqueous 2% nitric acid. The relative amount of iron per sample was then evaluated and correlated to the amount of CA per sample (n=5 per condition).

Subcutaneous (s.c.) in vivo biocompatibility studies of micropatterned PCL—

All surgical procedures were approved by the Institutional Animal Care and Use Committee (IACUC) of the Massachusetts General Hospital and performed according to the NIH Guidelines for the Care and Use of Laboratory Animals. The biocompatibility profile was evaluated for patterned PCL, patterned PCL spin-coated with CA, patterned PCL covered with 15 μ L of CA (n= 3 per formulation and time point). PCL disks, with a diameter of 7 mm, were disinfected by UV exposure overnight. Adult female Lewis rats (Charles River Laboratories, Wilmington, MA) were used in this study. General anesthesia was achieved with intramuscular injection of ketamine (38 mg/kg) and dexmedetomidine (0.1 mg/kg); 1 mg/kg antisedan was injected subcutaneously for the reversal of anesthesia. Six s.c. 1.5 cm long midline incisions were made on the back of each anesthetized animal. The patch coating procedure was performed in the operating room and the samples immediately, and randomly, implanted into the s.c. pockets. Animals were sacrificed at 1 and 3 weeks, and the implants and surrounding tissue harvested. Hematoxylin and eosin (H&E) and anti-CD68 stains were performed to characterize the inflammatory response.

In vivo functional studies—All surgical procedures were approved by the IACUC of the Massachusetts General Hospital and performed according to the NIH Guidelines for the Care and Use of Laboratory Animals. The use of flat and patterned CA spin-coated PCL patches to close defects requiring surgical repair was evaluated in colon and stomach perforations using a rat model. Adult female Lewis rats (Charles River Laboratories, Wilmington, MA) were used. All PCL patches tested were disinfected by UV exposure overnight. For both models, a defect was created using a 3 mm diameter dermal biopsy (Acuderm Inc.). Bleeding was controlled through compression and electro cauterization. For colon repair, 7-8 mm diameter flat or patterned patches were coated with a thin layer of CA and immediately applied to the defect. The degree of attachment was qualitatively evaluated by a blinded surgeon (n= 8 for flat samples, n= 11 for patterned samples). Animals whose colon defect was closed with a patterned spin-coated patch were survived for 1 week (n=6). H&E stain was used to evaluate the tissue response to the spin-coated patterned patch. For stomach repair, experimental groups included i. 7 mm diameter patterned spin-coated PCL patches (n=3), ii. A Graham patch that involved suturing the omentum over the defect (n=2), or iii. sham operated animals where the defect created was not closed (n=2). Animals were sacrificed at 2 weeks after the initial procedure. The degree of abdominal adhesions for each condition was evaluated and ranked from 0 (no adhesions) to 10 (extensive adhesions)

covering all abdominal cavity). H&E staining was used to evaluate tissue response to the different closure techniques.

Statistics—Data is expressed as means \pm standard deviation. The data was assumed to follow a Gaussian distribution and thus a one way anova was performed with Tukey's post-hoc analysis to examine statistical differences for: i. determining the effect of topography and CA amount on the adhesive strength of PDMS and PCL patch materials, ii. evaluating the s.c. biocompatibility of non-coated and coated PCL patches, iii. determining the degree of abdominal adhesion following stomach defect closure using multiple techniques. An unpaired t-test was used to compare the amount of CA glue retained on flat or patterned PCL surfaces following spin-coating. Data was assumed to be significant when a P-value was obtained either equivalent or less than 0.05.

Supplementary Material

Refer to Web version on PubMed Central for supplementary material.

Acknowledgments

We would like to thank Admet Inc. for generously providing an eXpert 7601 mechanical tester that was critical for this work. This work was also supported by the National Institutes of Health grant GM086433 to JMK, and National Institutes of Health grant DE013023 to RL. MJP acknowledges the Portuguese Foundation for Science and Technology (fellowshipSFR/BD/43013/2008) and the MIT-Portugal program (bioengineering focus area).

References

- [1]. Chang EI, Galvez MG, Glotzbach JP, Hamou CD, El-ftesi S, Rappleye CT, Sommer KM, Rajadas J, Abilez OJ, Fuller GG, Longaker MT, Gurtner GC. *Nat Med.* 2011; 17:1147. [PubMed: 21873986]
- [2]. Wang AA, Martin CH. *J Hand Surg.* 2003; 28A:696.
- [3]. Ciapetti G, Stea S, Cenni E, Sudanese A, Marraro D, Toni A, Pizzoferrato A. *Biomaterials.* 1994; 15:92. [PubMed: 8011865]
- [4]. Mizrahi B, Stefanescu C, Yang C, Lawlor M, Ko D, Langer R, Kohane D. *Acta Biomater.* 2011; 7:3150. [PubMed: 21569875]
- [5]. Vote BJT, Elder MJ. *Clin Exp Ophthalmol.* 2000; 28:437.
- [6]. Glass P, Cheung E, Sitti M. *IEEE Trans Biomed Eng.* 2008; 55:2759. [PubMed: 19126455]
- [7]. Mahdavi A, Ferreira L, Sundback C, Nichol J, Chan E, Carter D, Bettinger C, Patanavanich S, Chignozha L, Ben-Joseph E, Galakatos A, Pryor H, Pomerantseva I, Masiakos P, Faquin W, Zumbuehl A, Hong S, Borenstein J, Vacanti J, Langer R, Karp J. *PNAS.* 2008; 105:2307. [PubMed: 18287082]
- [8]. Kwak MK, Jeong HE, Suh KY. *Adv Mater.* 2011; 23:3949. [PubMed: 21796686]
- [9]. Artzi N, Shazly T, Baker AB, Bon A, Edelman ER. *Adv Mater.* 2009; 21:3399. [PubMed: 20882504]
- [10]. Park DH, Kim SB, Ahn KD, Kim EY, Kim YJ, Han DK. *J Appl Polym Sci.* 2003; 89:3272.
- [11]. Lee SH, Kim YT, Yang S, Yoon ES, Kim DE, Suh K. *ACS Appl Mater Interfaces.* 2010; 2:1308. [PubMed: 20415449]
- [12]. Lee H, Lee BP, Messersmith PB. *Nature.* 2007; 448:338. [PubMed: 17637666]
- [13]. Ng K, Achuth H, Moochhala S, Lim T, Hutmacher D. *J. Biomat. Sci. Polym. E.* 2007; 18:925.
- [14]. Kim DS, Lee BK, Yeo J, Choi MJ, Yang W, Kwon TH. *Microelectronics Eng.* 2009; 86:1375.
- [15]. Roy S, Ansari KJ, Jampa SSK, Vutukuri P, Mukherjee R. *ACS Appl. Mater. Interfaces.* 2012; 4:1887. [PubMed: 22468781]

- [16]. Siu WT, Leong HT, Law BKB, Chau CH, Li ACN, Fung KH, Tai YP, Li MKW. *Ann Surg.* 2002; 235:313. [PubMed: 11882751]
- [17]. Shah S, Lowery E, Braun RK, Martin A, Huang N, Medina M, Sethupathi P, Seki Y, Takami M, Byrne K, Wigfield C, Love RB, Iwashima M. *Plos One.* 2012:7.
- [18]. Nursal TZ, Anarat M, Bircan S, Yildirim S, Tarim A, Haberal M. *Am J Surg.* 2004; 187:28. [PubMed: 14706582]

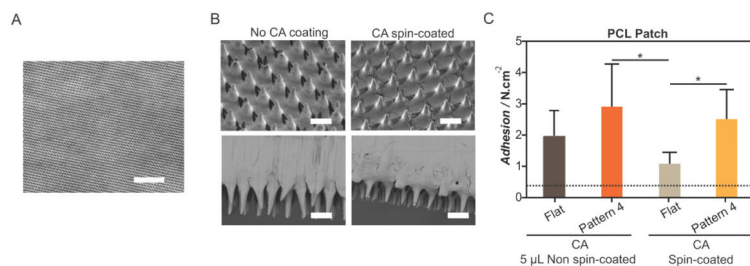


Figure 1. Surface topography combined with CA coating significantly enhanced the adhesion force of PCL patches on wet *ex vivo* intestine tissue. A) Large PCL surface areas were reproducibly patterned through hot embossing. Scale bar 100 μm . B) PCL patterned surfaces (whole and fracture surface samples) before and after spin-coating with CA as imaged by SEM. Scale bars 10 μm . C) Pull-off adhesion forces for coated PCL patches ($n = 6$ per condition, each n is an average of 3 technical replicates). No differences in adhesion were observed when an excess of CA (5 μL) was applied to flat versus patterned surfaced (non spin-coated). However, topography enhanced the adhesion force of CA spin-coated samples, with more than double the level of adhesion obtained for CA sin-coated patterned substrates compared to CA flat spin-coated samples. The adhesion force for a flat or patterned PCL substrate without CA coating was approximately 0.3 N/cm^2 (dotted line).

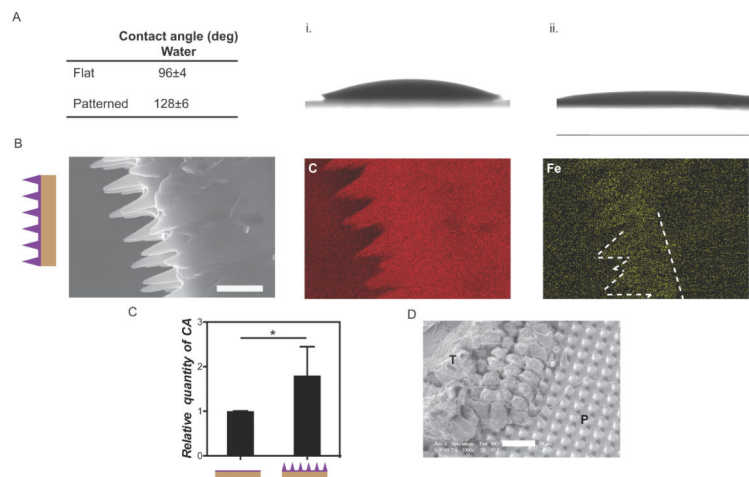


Figure 2.

Characterization of CA coated surfaces. A) Contact angles of water and CA on flat and patterned PCL samples. B) Lower CA spreadability was observed on flat (i) than on (ii) patterned substrates. C) Cross-section of CA spin-coated films on patterned PCL. Chemical mapping of IO nanoparticles encapsulated within CA demonstrated that CA covered the patterned area. Scale bar 10 μm . D) Quantification of CA on flat and patterned spin-coated PCL patches through ICP-AES ($n=5$ per condition). The CA amounts on spin-coated flat substrates were 13 ± 2 times less than 5 μL (non spin-coated) CA coated substrates (data not shown). E) SEM image of patterned PDMS after adhesion testing against *ex vivo* intestine tissue. Tissue residue (T) was visible on the patch surface and was interlocked with the surface topography (P). Scale bar 20 μm .

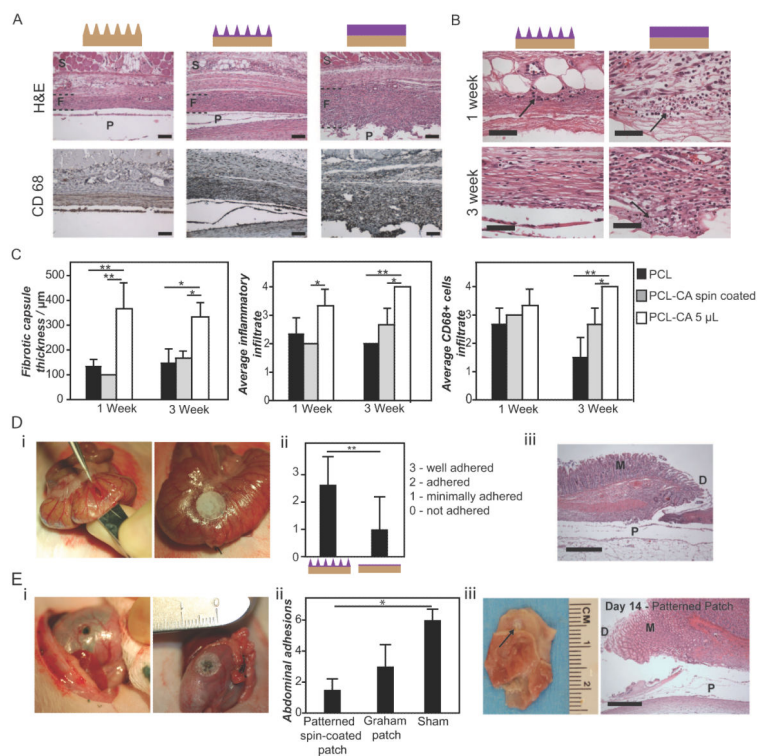


Figure 3. pin-coated CA on micro-patterned PCL generated minimal tissue inflammatory and toxic responses, while assuring strong tissue adhesion to seal stomach and colon perforations. A) H&E staining of the tissue surrounding the adhesive patch, 3 weeks post-subcutaneous implantation in a rat; the adhesive layer was positioned towards the skin (S: skin, F: fibrotic capsule, P: polymer implant). Scale bar 100 μ m. B) Cell necrosis (arrows) was observed 1 week post-implantation in all CA containing samples; however, necrosis was found only in 5 μ L CA samples 3 weeks post-implantation. Scale bar 50 μ m. Arrows point to locations of cell necrosis. C) After 1 and 3 weeks implantation, chronic inflammation was characterized (n= 3 per formulation and time point) based on the fibrotic capsule thickness surrounding the patterned implant, the inflammatory infiltrate, and the density of CD68+ cells (0-negligible to 4-severe). D) i. Images of a 3 mm diameter defect in the rat colon before and after closure with a CA spin-coated patterned PCL patch. ii. Adherence of CA spin-coated patterned and flat PCL patches to the colon, evaluated upon patch placement by a single surgeon blinded to patch topography (n= 8 for flat samples, n= 11 for patterned samples). iii. H&E stained sections of colon defects 1 week post-implantation (P: patch, M: mucosa, D: defect). The inflammatory response was moderate. E) i. Images of a 3 mm diameter defect in the rat stomach before and after closure with a CA spin-coated patterned PCL patch. ii. Abdominal adhesions (0 – 10 for no to severe adhesions covering the abdominal space) 2 weeks post-repair with patterned spin-coated patch (n=3), graham patch (n=2), or without surgical repair (sham, n=2). iii. Macropathology and H&E stained sections of stomach defects with CA spin-coated patterned PCL patches 2weeks post-repair (P: patch, M: mucosa, D: defect). The CA spin-coated PCL patch did not interfere with repair of stomach

mucosa. Minimal to moderate tissue inflammation was observed based on histological analysis.